Detecting soil salinity with arid fraction integrated index and salinity index in feature space using Landsat TM imagery

Fei WANG[1,2], Xi CHEN[1], GePing LUO[1], JianLi DING[3*], XianFeng CHEN[1,4]

[1] State Key Laboratory of Desert and Oasis Ecology, Xinjiang Institute of Ecology and Geography, Chinese Academy of Sciences, Urumqi 830011, China;
[2] University of Chinese Academy of Sciences, Beijing 100049, China;
[3] College of Resources and Environmental Science, Xinjiang University, Urumqi 830046, China;
[4] Slippery Rock University of Pennsylvania, Slippery Rock, PA16057, USA

Abstract: Modeling soil salinity in an arid salt-affected ecosystem is a difficult task when using remote sensing data because of the complicated soil context (vegetation cover, moisture, surface roughness, and organic matter) and the weak spectral features of salinized soil. Therefore, an index such as the salinity index (SI) that only uses soil spectra may not detect soil salinity effectively and quantitatively. The use of vegetation reflectance as an indirect indicator can avoid limitations associated with the direct use of soil reflectance. The normalized difference vegetation index (NDVI), as the most common vegetation index, was found to be responsive to salinity but may not be available for retrieving sparse vegetation due to its sensitivity to background soil in arid areas. Therefore, the arid fraction integrated index (AFII) was created as supported by the spectral mixture analysis (SMA), which is more appropriate for analyzing variations in vegetation cover (particularly halophytes) than NDVI in the study area. Using soil and vegetation separately for detecting salinity perhaps is not feasible. Then, we developed a new and operational model, the soil salinity detecting model (SDM) that combines AFII and SI to quantitatively estimate the salt content in the surface soil. SDMs, including SDM1 and SDM2, were constructed through analyzing the spatial characteristics of soils with different salinization degree by integrating AFII and SI using a scatterplot. The SDMs were then compared to the combined spectral response index (COSRI) from field measurements with respect to the soil salt content. The results indicate that the SDM values are highly correlated with soil salinity, in contrast to the performance of COSRI. Strong exponential relationships were observed between soil salinity and SDMs (R^2>0.86, RMSE<6.86) compared to COSRI (R^2=0.71, RMSE=16.21). These results suggest that the feature space related to biophysical properties combined with AFII and SI can effectively provide information on soil salinity.

Keywords: soil salinity; spectrum; halophytes; Landsat TM; spectral mixture analysis; feature space; model

Only considering soil reflectance may not be enough to measure variation in soil salinity because of the influence of the complicated soil context (surface roughness, organic matter and moisture) (Metternicht and Zinck, 2003). Therefore, to avoid the limitations of soil reflectance, some studies have introduced vegetation as an indirect indicator to determine soil salinity over a local area (Dehaan and Taylor, 2002). As a remotely sensed indicator, the type and growing conditions of vegetation can provide a spatial overview of salinity distribution (Tilley et al., 2007). Vegetation reflectance has been studied to determine

the response to certain factors, including ozone, pathogens, senescence, and dehydration (Carter, 1993). The increased visible reflectance (VIS) and the reduced near-infrared reflectance (NIR) have been found to be a consistent measure of chlorophyll reduction and cell structure damage among various species in response to stress (Carter, 1993). These changes in VIS and NIR were also found in the response to salt stress (Tilley et al., 2007). Soil salinity has been estimated in numerous studies by using vegetation reflectance, and many of these studies preferred the use of vegetation indices, especially the normalized difference vegetation index (NDVI) (Tilley et al., 2007).

The above studies also researched the response of NDVI to soil salt but did not consider soil and vegetation simultaneously. Therefore, Fernandez-Buces et al. (2006) used a modified NDVI to acquire a high correlation with salinity (R^2>0.8) in a semi-arid area in Mexico. Although the progress in detecting soil salinization has been made, the predictive power of this approach has not been examined in other locations, such as an arid region. Moreover, NDVI is sensitive to the optical properties of soil and is difficult to interpret with sparse information on the vegetation (such as vegetation cover) in an arid area. Therefore, a number of derivatives and alternatives to NDVI have been proposed to address this limitation, such as the soil-adjusted, modified soil-adjusted and optimized soil-adjusted vegetation indices (SAVI, MSAVI and OSAVI, respectively). Although vegetation indices such as the SAVI considerably reduce inconsistencies, this method still suffers from some limitations, especially at relatively low vegetation cover (Rondeaux et al., 1996), if no information about the target is known. Nevertheless, according to the results of some studies, NDVI is an appropriate index to estimate the vegetation cover fraction where crops are concerned (Wardlow and Egbert, 2008; Yang et al., 2011), but it is not appropriate for shrub lands and grasslands due to the effect of mix-pixel (Montandon and Small, 2008), especially soil components at a sub-pixel level. Spectral mixture analysis (SMA) has often been implemented to address the problem of mixed pixels and has been promoted as an effective method of deriving the vegetation cover from multispectral imagery in arid areas (Jiapaer et al., 2011). Therefore, the arid fraction integrated index (AFII), which incorporates the fractions of bare soil and vegetation obtained from SMA, was developed to estimate the vegetation cover in arid lands.

The salinity index (SI), which combines the blue and red band, is sensitive to the surface reflectance of salt-affected land with spare vegetation cover (Douaoui et al., 2006). We used SI along with AFII to simultaneously detect soil salinity. To utilize the synergistic relationship between soil and vegetation, we employed the concept of two-dimensional feature space to determine the response of this relationship to soil salinity. A number of studies have documented that two-dimensional feature space has a potential to permit the retrieval of soil moisture, air temperature, fire detection, evapotranspiration, land cover classification, and desertification monitoring based on different relationships, such as LST (Land surface temperature) and VI, LST and Albedo (Yang and Wang, 2011), surface-air temperature and VI (Gillies et al., 1997), Red and NIR (near-infra-red) (Ghulam et al., 2007a), NDVI and Albedo (Ghulam et al., 2007b), and others. However, there are few studies on soil salinization detection based on two-dimensional feature space in arid areas.

The purpose of this study was to develop a methodology to detect soil salinity in the Kuqa River delta. A Landsat 5 Thematic Mapper (TM) image was used to: (1) develop an AFII index that incorporates SMA to extract vegetation fraction; (2) examine the relationship between AFII and SI in response to the variation in soil salt content; and (3) construct a soil salinity detecting model (SDM) that integrates AFII and SI in feature space.

1 Materials and methods

1.1 Study area

Covering approximately 2,500 km^2, the study area is between 83°01′–83°37′E and 41°23′–42°50′N in the north fringe of the Taklimakan Desert, Xinjiang Uygur autonomous region, China. It is located in the northeast of the delta oasis of the Kuqa River (Fig. 1). The area has an extremely arid desert climate with a mean

annual precipitation of 51.6 mm, a mean potential annual evapotranspiration of 2,723.7 mm, and an annual accumulated temperature (>10°C) of 4,500°C.
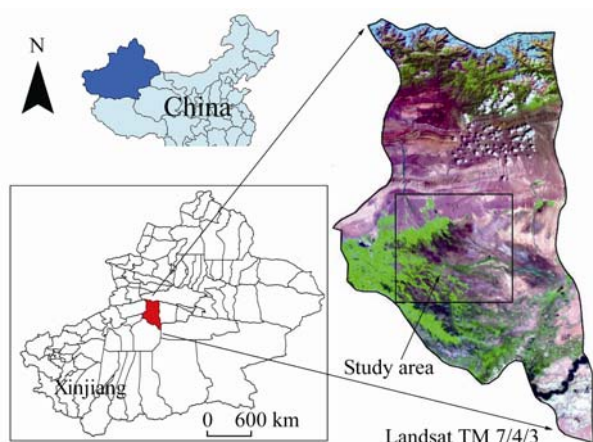

Fig. 1 Location of the study area

With plenty of runoff and groundwater from the mountains, the oasis of the Kuqa River establishes itself in a river delta, on the edge of diluvial-alluvial fans and alluvial-diluvial plains, and thus a green ring forms by the oasis around the edge of the Tarim Basin. The topographic elevation in this area ranges from 920 to 1,100 m, decreasing from northwest to southeast. The soil types in the study area include agricultural anthrosols with low salinity (soils that human activities have resulted in profound modification to their properties) in the upper part of the oasis, orthic solonchak with low albedo (dark topsoil with a thick crust due to changes in the accumulation of salt content after evaporation) in the upper-middle part of the oasis and solonchaks with high albedo (white and strongly salinized soils formed by a continuous increase of salt content) in the lower part of the oasis.

Agricultural land along the Kuqa River has expanded drastically to provide for the growing population, especially during the last 50 years. Irrigation and backward drainage systems have caused over 10% of the total land area of the oasis to become salinized, and have subsequently accelerated a rise in the level of groundwater. Groundwater levels fluctuate by at least 2–3 m in depth, and the water in this part of the surface aquifer system is highly mineralized. Strong surface evaporation of water and transpiration by

plants has resulted in the salt accumulation in the root zone or at the soil surface because of capillary rise, leading to the formation of crusts. As a result, salt content in the surface soil (0–10 cm) is 0.6%–1.0% in some localized areas and even 2% in the low-lying area when including surface salt crusts (Zhang et al., 2012). Therefore, the stability of these areas which are threatened by serious soil salinization, is very low (Luo et al., 2009).

The vegetation types include halophytes and crops. The major halophyte communities are characterized by *Nieraria langutorum*, *Halostachys caspica*, *Phragmites australis*, *Alhagi sparsifolia*, *Karelinia caspica*, and *Kalidium gracile*, which grow well in the moderately and lightly salinized soils and have an average cover of 30% as shown by field surveys.

1.2 Data

1.2.1 Remote sensing imagery

A Landsat 5 TM image covering the study area (Path 145, Row 31) for 25 July 2007 was acquired. For the quantitative inverse analysis of surface variables, removing the influence of the atmosphere is a critical pre-processing step. The TM data were geometrically corrected, and digital numbers were converted into radiances. Then, the ENVI FLAASH (fast line-of-sight atmospheric analysis of spectral hypercube) model was employed for correcting atmospheric effects, and the MODTRAN (moderate resolution atmospheric transmission) was used as the atmospheric radiation correction model with high precision. The values of reflectance were determined last.

1.2.2 Field investigation

Samples were collected according to a systematic, random sampling design in the salt-affected soils according to previous work in the study area (Jiang et al., 2008). Each sampling plot covers an area of 900 m². A total of 62 samples (soil and vegetation cover) were measured during a field survey carried out at the time of the Landsat acquisition. At each sampling plot, five soil samples were taken. Vegetation (crops and halophytes) cover was measured within each 900-m² sampling plot. In the laboratory, the composite soil samples were air-dried, ground and sieved through a

2-mm sieve and then analyzed for soil salt content. Individual spectral measurements were the average of 5–10 scans of bare soil, and each canopy was generally sampled 10 or more times. These samples were then averaged to provide a single spectrum for each target. Figure 2 shows the field-derived average spectra of salt-affected soils and vegetation. Halophye has relative sparse canopies compared to crops and consequently has lower reflectance across the visible spectrum. The average reflectance of halophytic vegetation is higher than that of crops at 560 nm due to active excretion of the salt excess by salt glands on leaf surfaces. This result is similar to that found by Zhang et al. (2012).
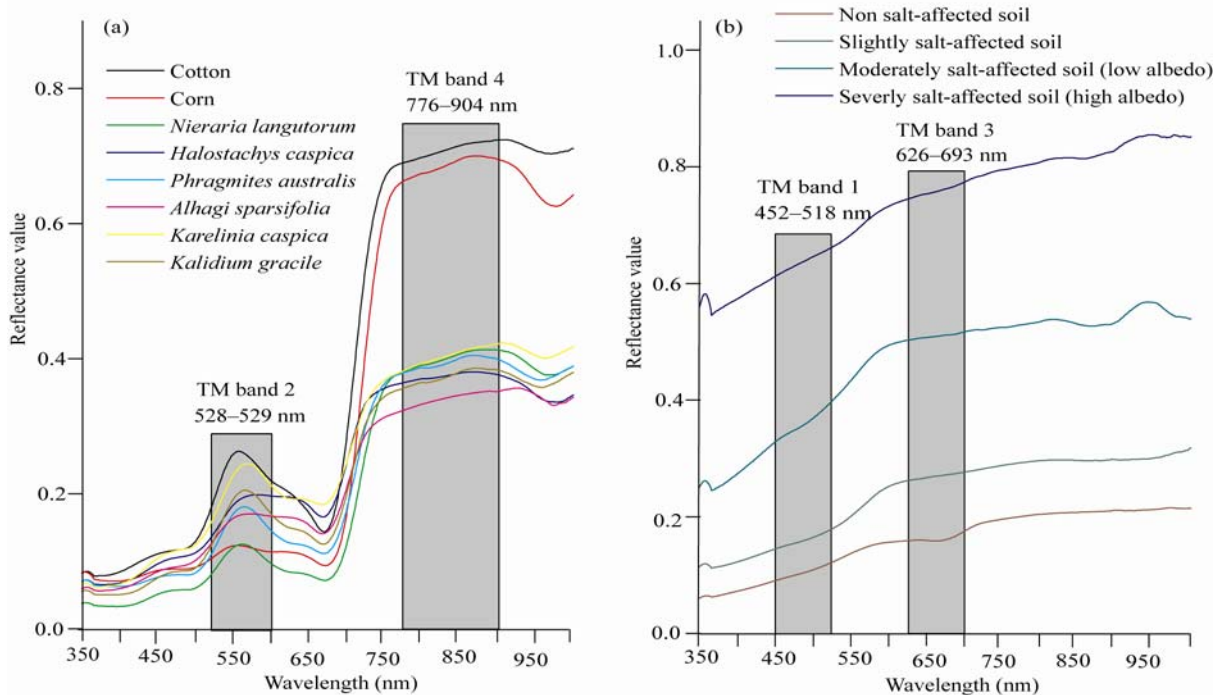

Fig. 2 Field-derived average spectra of salt-affected soils and vegetation. (a) Spectral responses to salt stress can be classified as two classes (crops and halophytes). Cotton and corn produced a similar shape, with lower reflectance in the green region (528–609 nm, particularly at 560 nm) and higher reflectance in the NIR (nearinfra-red) region (776–904 nm) compared to halophyte. (b) Reflectance of various salt-affected soils without saline crusts.

1.3 Methodology

As soil salinity levels become more extreme, the growth response of the vegetation is greatly affected. As the soil salt content increased, vegetation diversity decreased (Bui and Henderson, 2003; Fernandez-Buces et al., 2006), soil surface temperature increased, and soil moisture and soil evapotranspiration decreased when a salt crust was present (Mougenot et al., 1993), which resulted in an increase in soil reflectance. This study proposed a soil salinity detection model (SDM) derived from remote sensing data and related to two indicators, AFII and SI.

Figure 3 shows a flow chart describing the major steps in the methodology used to monitor soil salinity. First, AFII was established from spectral mixture analysis (SMA) and evaluated by comparison with field data. During this step, the soil and vegetation factors that were obtained from SMA were considered in AFII.

Subsequently, the SDM was constructed by analyzing the scatter trajectory feature in AFII-SI space and its biophysical process. Finally, the study evaluated the performance of SDM compared with the
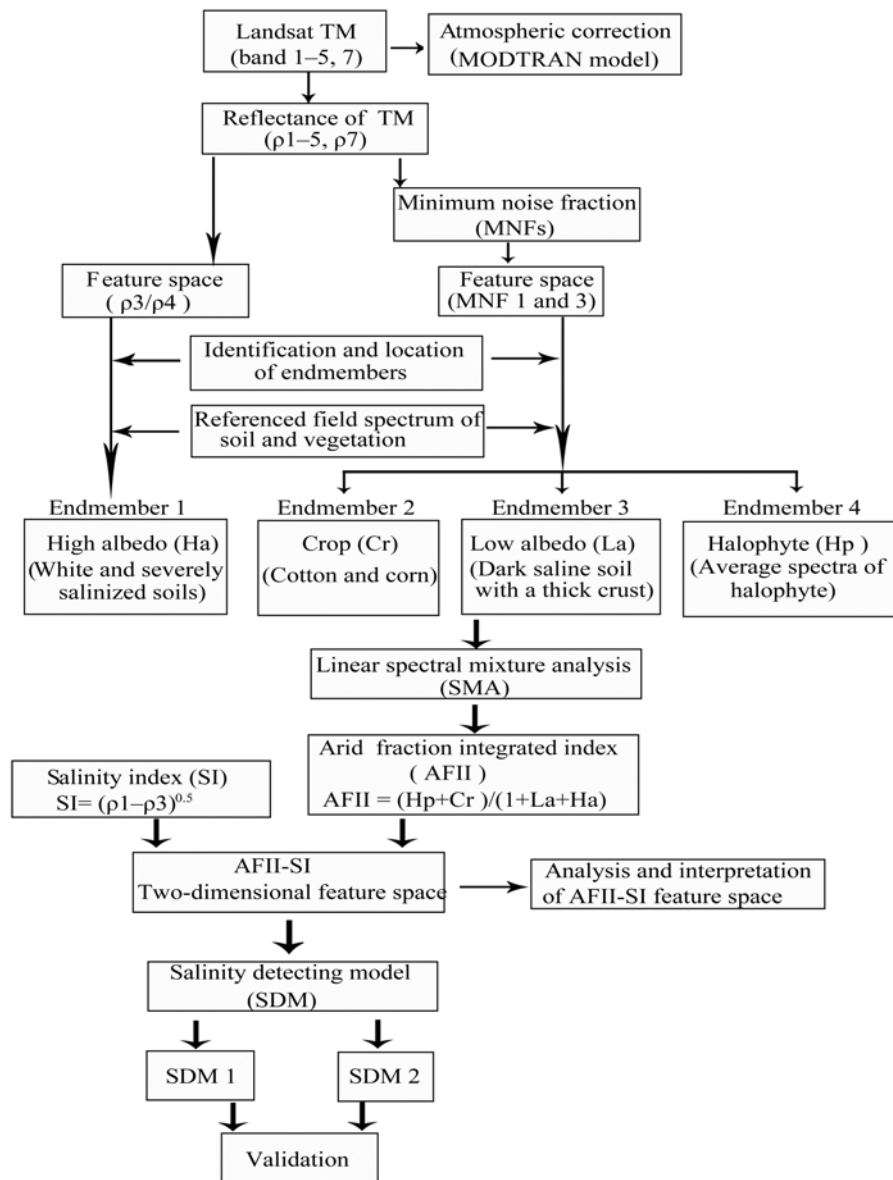
Fig. 3 Flow chart of soil salinity detection methodology proposed using two indices, AFII, related to vegetation (crops and halophytes) cover, and SI, related to soil brightness in the salt-affected soil area. AFII is developed from the relationship among the fractions of crops, halophytes, dark soil and light soil that derives from SMA. The SDM (soil salinity detecting model) was constructed from the two indices based on the two-dimensional feature space and was evaluated by measured data.

Combined Spectral Response Index (COSRI) based on the measured data (Fernandez-Buces et al., 2006). The COSRI was calculated for bare soil and vegetation by adjusting the NDVI to predict soil salinity.

1.3.1 Establishment of AFII

SMA has often been used to address the problem of mixed pixels. This approach decomposes each pixel in an image into a linear component of a reference spectrum, referred as endmembers. This spectrum can be either developed from laboratory or field spectra or derived directly from image data. The linear spectral unmixing model (Vandermeer, 1995) is by far the most common type of SMA, and although it is theoretically imperfect due to the omission of the effect of multiple scattering between cover types, the errors associated with the linear assumptions have been

found to be relatively minor. Linear SMA models have also been proven to be reasonably effective in estimating endmember fractions and are widely used due to their simplicity, reasonable effectiveness and interpretability (Xiao and Moody, 2005). SMA provides a method for determining the fraction of plant and soil within a pixel, without effective limitations on the number of bands. Different soil types or backgrounds can be parameterized adequately based on SMA to quantitatively decrease the influence of soil on plants in a mixed pixel.

Because of the existing correlation between bands, the intrinsic spectral dimensionality of a multispectral image is usually lower than the number of image bands. This is especially true for the Landsat TM and ETM+ instruments, where the bands in the visible domain are highly correlated. Therefore, only four or

five endmembers can be supported (Small and Lu, 2006).

To reduce the number of endmembers and ensure that the SMA algorithm is effective, the modified normalized difference water index (MNDWI) (Xu, 2006) and NDVI were used to delete pixels that included water bodies and Gobi desert. The key to successful SMA is appropriate endmember selection. Determination of endmembers involves identifying the number of endmembers and extracting their corresponding spectral signatures.

Four endmembers were selected, including high albedo, low albedo, crops, and halophytes (Fig. 4). The minimum noise fraction (MNF) algorithm (Green et al., 1988) was applied to the image of the study area in that the MNF-transformed data were used as input to determine the most spectrally pure pixels in the
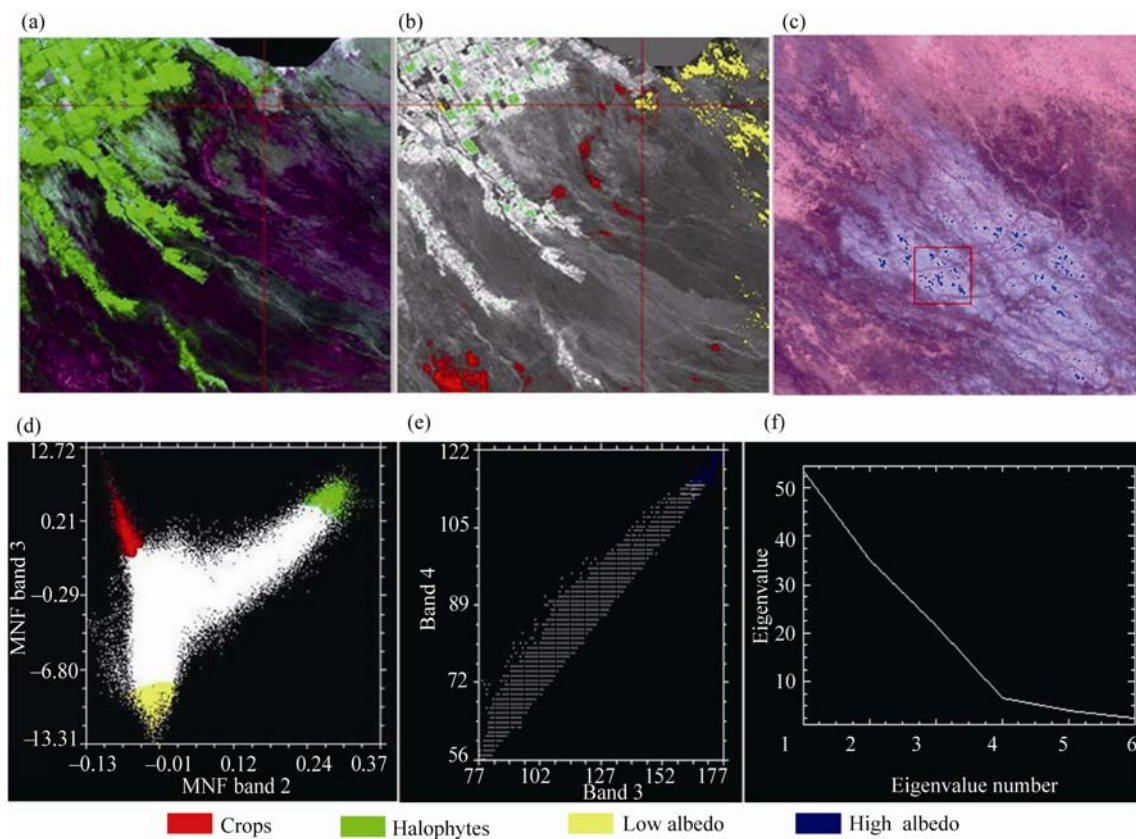

Fig. 4 Extraction of representative soil and vegetation endmembers of the study area with minimum noise fractions (MNFs) (first and third MNF) and RED-NIR feature space. (a) The false color composite images (bands 3–5); (b) map of NDVI with green, red and yellow colors indicating areas with farmland, bare soil (low albedo) and high-density halophytes; (c) false color composition images of halophytes (bands 3–5) with blue pixels covered by white and strongly salinized soils (high albedo); (d) determining the locations of the three endmembers (crops, halophytes and low albedo) in MNFs 1 and 3 feature space; (e) determining the location of high albedo in RED-NIR feature space; (f) the MNF band's eigenvalues showing most information accounted for by the first three MNFs.

image. Low albedo, halophyte and crop endmembers were extracted according to a feature space representation constructed with the first and third components of MNF (Fig. 4c). In this study, crop endmembers consist of cotton and corn. Halophyte endmembers consist of *Nieraria langutorum*, *Halostachys caspica*, *Phragmites australis*, *Alhagi sparsifolia*, *Karelinia caspica*, and *Kalidium gracile*, which can be used as the training endmembers for SMA because of their similar shape and reflectance value (Fig. 2a). Low albedo primarily consists of typic solonchak containing dark topsoil with a thick crust (Fig. 1d). The two-dimensional feature space plot between the RED and NIR bands was also used for the selection of endmembers (Peterson and Stow, 2003). The upper-right apex is characterized by bright soil with high reflectance values (Figs. 4d and e). We did not specially process the shadow/shaded problem in this analysis because there is little impact from solving mixed spectra among the endmembers. The spectral signatures of all selected endmembers are shown in Fig. 5 and are similar to the field spectral measurements (Fig. 2).
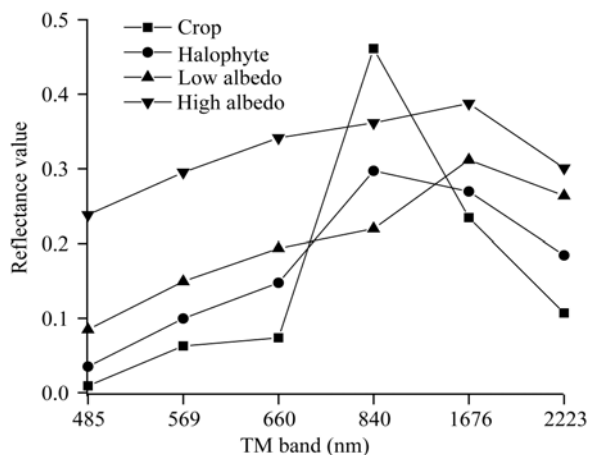

Fig. 5 Spectral curves of selected endmembers

AFII was established to interpret the vegetation cover. An algorithm was built by the hypothesis that the presence and proportion of vegetation, particularly halophytes, implied different degrees of soil salinization (Dehaan and Taylor, 2002). AFII is an index to measure the abundance of vegetation cover within a 30 m×30 m pixel. Through utilizing this concept, we made use of the fractional abundance of vegetation and soil to define AFII on a pixel-by-pixel basis as follows:

$$AFII = \frac{f_{hv} + f_{cr}}{1 + f_{la} + f_{ha}}. \tag{1}$$

Where f_{hv}, f_{cr}, f_{la} and f_{ha} are the fractions of halophytes, crops, low albedo and high albedo, respectively. The addition of 1.0 in the denominator limits AFII from 0 to 1, with high values indicating high vegetation cover, and lower values correspondent to high ground cover. Using the above equation, the coverage of sparse vegetation may be estimated in the study area.

1.3.2   Spectral response of salt-affected soil

Alterations of chemical equilibria and loss of soil fertility are concomitant with structural degradation, which results in salt crusts, especially in salt-affected areas. Salt-affected soils have been found to reflect more incident radiation on the visible spectrum (0.45–0.68 μm) than salt-unaffected land cover features (Khan et al., 2005). This response of saline soils is extremely useful as it helps the segregation of different salt-affected soils. With respect to the spectral reflectance of individual bands appropriate for salt-affected soils, various combinations were tested for the Landsat TM sensor, but SI performed best at low surface moisture content (Douaoui et al., 2006). Figure 2 shows the reflectance of band 1 and band 3 of the Landsat 5 TM with various salt-affected soils in the study area. These results are similar to those in previous works (Khan and Sato, 2001). SI equation is expressed as follows:

$$SI = \sqrt{\rho_1 \times \rho_3}. \tag{2}$$

Where ρ_1 and ρ_3 are the reflectance of band 1 and band 3 of the Landsat, respectively.

1.3.3   Construction of SDM

Figure 6a shows the conceptual diagrams of different salinized soils in AFII-SI feature space. Within the AFII-SI space along the x-axis, AFII increases due to better vegetation cover, while along the y-axis, SI increases, reflecting a rise in salt content in the surface soil. Such a combination can contribute to land cover mapping and land cover change analysis in the AFII-SI space, which contains information on many
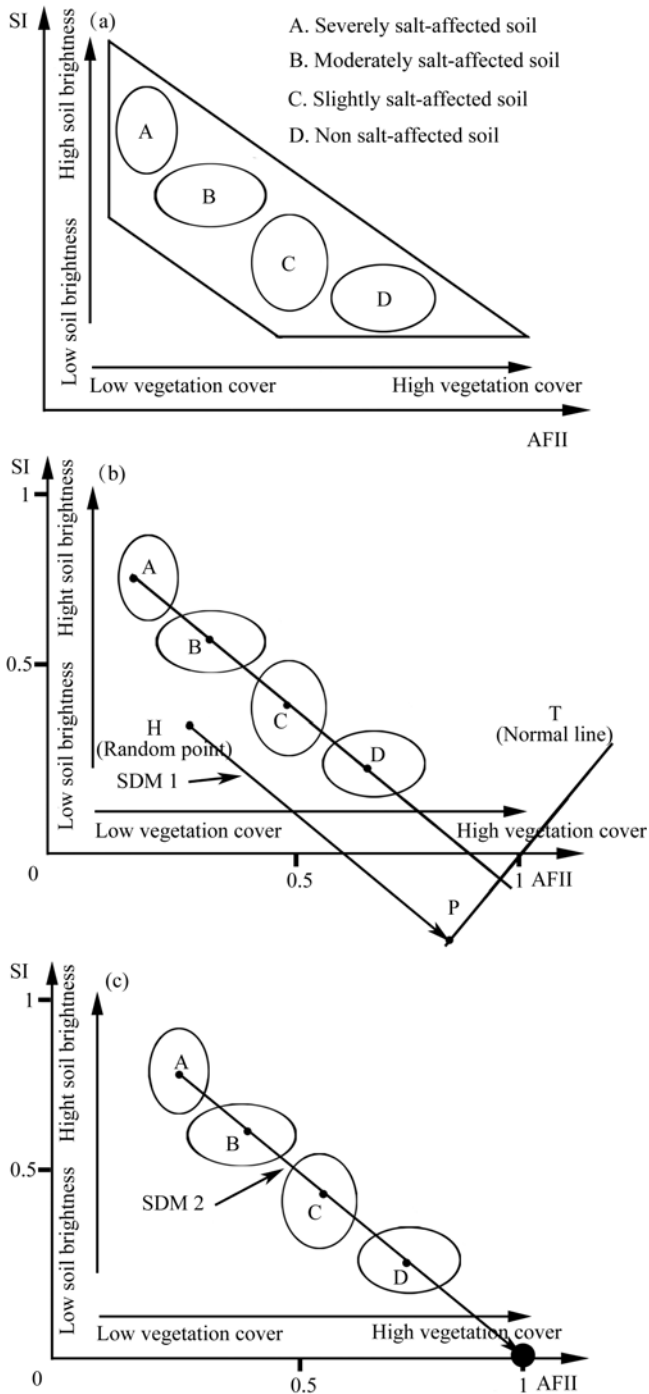
Fig. 6 Conceptual diagram showing the expected relationship between AFII and SI in salt-affected soil. For illustrating the soil salinization concept, four ellipses have been drawn. (a) Severely salt-affected soil A is considered to have high SI and low AFII. Only a few high-tolerance halophytes can survive in this soil. Moderately salt-affected soil B is considered to be in the areas that are occupied by halophytes and dark soil. Slightly salt-affected soil C is considered to be in areas with high crop cover and few halophytes present, resulting in high AFII and low SI. Non salt-affected soil D is covered by farmland. (b) and (c) are the sketch maps of salinity detecting model (SDM)1 and SDM2.

biophysical attributes and processes of soil salinization. Figure 6 illustrates the conception of the soil salinization process. Here, the AD line represents the direction of soil salinization from severely salt-affected soils to moderately salt-affected soils, slightly salt-affected soils and non salt-affected soils, which can be expressed by the following equation:

$$SI = K \times AFII + C. \tag{3}$$

Where K refers to the slope of AD, and C is the interception on the vertical axis.

A line T that crosses the coordinate (1, 0) and is vertical to the line AD can be delineated in Fig. 6b. Therefore, as the normal function of a line, T can be mathematically formulated from the AD equation:

$$SI = -\frac{1}{K} AFII + 1. \tag{4}$$

With an increasing amount of vegetation, the plot shifts upward vertical to line AD, while with a decrease in the soil salt content, the plot shifts parallel to line AD and orthogonal to normal line T. That is, the farther the distance from T, the stronger the soil salinization. Therefore, it is possible to determine the soil salinity using the mathematical expression of the distance from the appropriate point to line T. Taking a random point in the AFII-SI space, H (X_{AFII}, Y_{SI}), the distance indicated by SDM1 from H (X_{AFII}, Y_{SI}) to line T, can be calculated using the following:

$$SDM1 = \left| \frac{KY_{SI} + X_{AFII} - 1}{\sqrt{1 + K^2}} \right|. \tag{5}$$

Therefore, pixels placed near line T are always crop land (low saline) which infinitely approaches 0; while the area farthest from line T represents an extremely salinized soil surface.

Figure 6c shows another, simpler conception compared to Fig. 6a. Taking a random point H (X_{AFII}, Y_{SI}) in the AFII-SI space, the distance represented by SDM 2 from the point (1.0) indicates a different salinity condition. The farther the distance from the point (1.0), the stronger the soil salinization. The SDM2 can be expressed by the following equation:

$$SDM2 = \left[\left(X_{AFII} - 1 \right)^2 + Y_{SI}^2 \right]^{\frac{1}{2}}. \tag{6}$$

1.4   Validation

The resulting actual measured soil salt contents and

vegetation covers of the samples were then compared with their predicted values from sample TM pixels to evaluate the different models. A coefficient of determination (R^2) was used to assess the accuracy of this method. We also compared the models by computing the root mean square error (RMSE), as shown below:

$$R^2 = 1 - \sum_{i}^{n}\left(Y^` - Y\right)^2 / \sum_{i}^{n}\left(Y^` - \overline{Y}\right)^2. \qquad (7)$$

$$RMSE = \sqrt{\frac{1}{N}\sum_{i}^{n}\left(Y - Y^`\right)^2}. \qquad (8)$$

Where $Y^`$ and Y are the measured and predicted values, respectively, $\overline{Y}$ is the mean of the observed values, and n is the number of observations.

2 Results

2.1 Responses of vegetation cover to salt stress

Soil salinization is categorized into four classes: severe salinization, moderate salinization, slight salinization and non salinization according to the soil salt content and plant salt-tolerance capacity. The characteristics of each soil category are described in Table 1. The degree of soil salinity as a selection mechanism characterizes a relationship that is exemplified by lower vegetation cover or diversity in response to higher soil salt stress in the study area, and vice versa (Table 1). A relatively strong correlation between vegetation cover and soil salt content, an R^2 greater than 0.74, was found according to regression analysis (Fig. 7). This preliminary result indicates that determination of the vegetation fraction might be a useful tool to detect soil salinity.
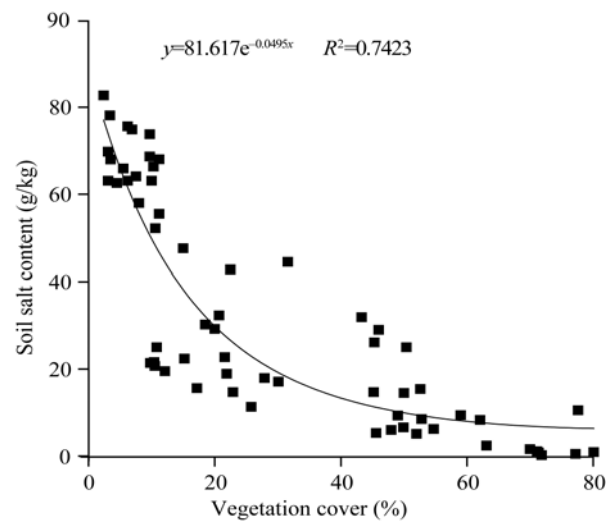

Fig. 7 Correlation between soil surface salt content and total vegetation cover in the study area; n=62

2.2 Performance of AFII

Figure 8 shows the distribution of vegetation derived from an image using two vegetation indices, AFII and NDVI. A high abundance of vegetation is indicated by a bright tone and a low abundance by a darker tone. The distribution of halophytes and crops, revealed by AFII, is concentrated in the northwest and southwest, but NDVI is only good at indicating irrigated land. Sparse vegetation is clearly observed at low elevations when using AFII (Fig. 8a) compared to NDVI (Fig. 8b) in the northeast, and especially in the southeast. Visual examination confirmed the ability of AFII and NDVI to retrieve vegetation information, and an accuracy assessment was also carried out using the field measured data.

Table 1 Primary characteristics of the salt-affected soil classification categories, in terms of soil salt content and vegetation cover according to He et al. (2006)

| Category	Characteristics
Severely salt-affected soil	High soil salt content (SSC>75 g/kg); low total vegetation cover (0–3%); few halophytes survive
Moderately salt-affected soil	Moderate soil salt content (45 g/kg<SSC<75 g/kg); moderate total vegetation cover (3%–15%); few types of halophytes survive
Slightly salt-affected soil	Light soil salt content (15 g/kg<SSC<45 g/kg); total vegetation cover ranging from 15% to 50%; various types of halophytes survive
Non salt-affected soil	Low soil salt content (SSC<15 g/kg); total vegetation cover ranging from 55% to 100%; crops dominate
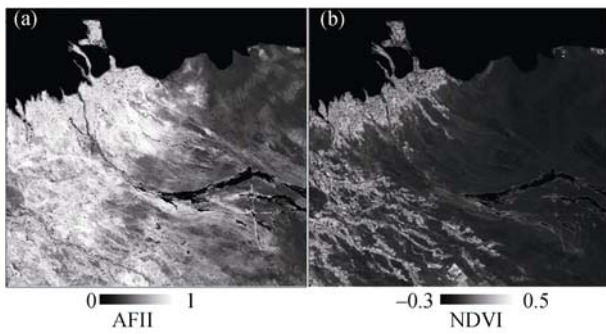
Fig. 8 Distribution of vegetation indices. (a) AFII, (b) NDVI. The whiter the color, the higher the proportion of vegetation cover is within the pixel. The dark areas mask water bodies and Gobi desert.
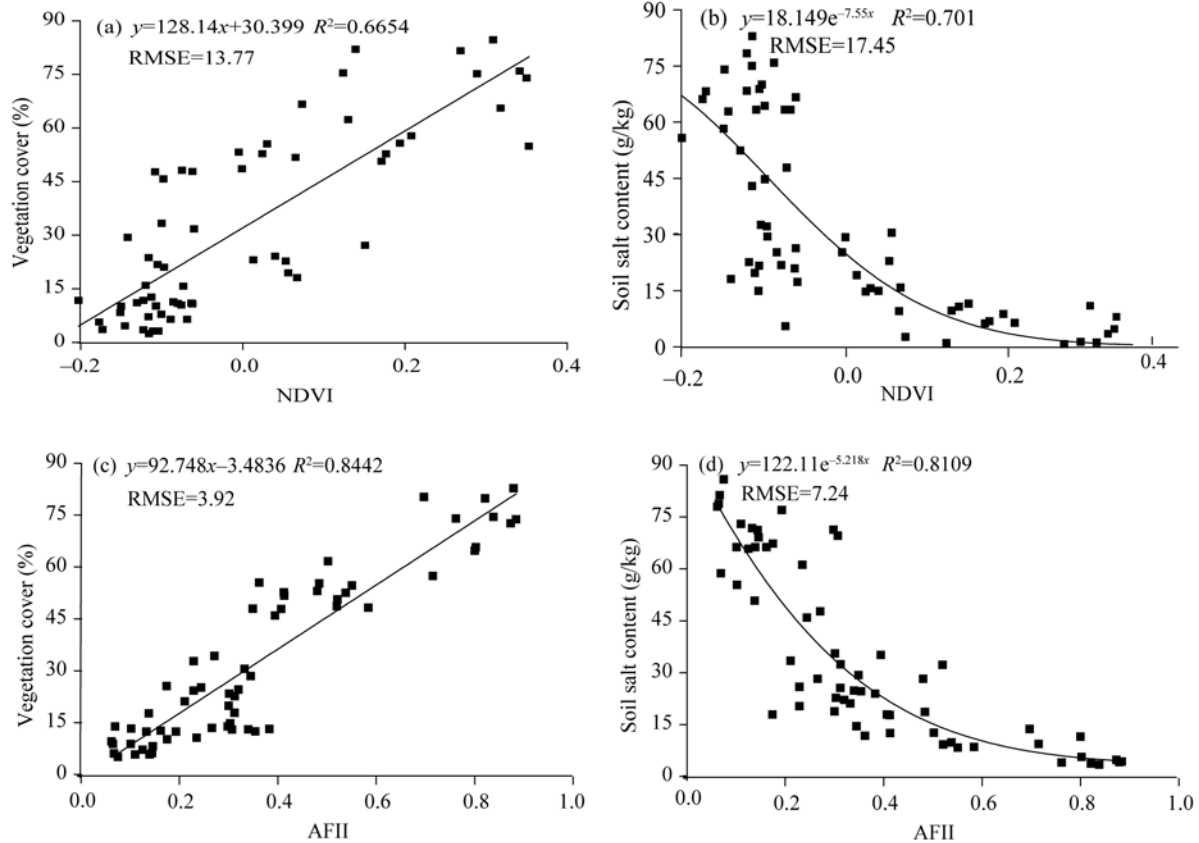
A total of 62 plots were sampled to estimate the accuracy of AFII. NDVI was compared to AFII. The regression analysis for NDVI achieves a relatively low positive goodness of fit (R^2=0.67), whereas that for AFII obtains a higher goodness of fit (R^2=0.84) and a lower RMSE (Figs. 9a and c). Assessing the soil salt content with AFII and NDVI exhibits similar trends to those mentioned above, but a different relationship was found, linear for vegetation and exponential for soil salt content. AFII outweighs NDVI in estimating soil salt content (Figs. 9b and d). AFII achieves a slightly higher coefficient of determination (R^2=0.75) and a notably lower RMSE of 7.3 compared to the results of NDVI with salinity (R^2=0.70, RMSE=17.5).

Fig. 9 Regression relationship between the vegetation index and field data. (a) NDVI vs. VC (vegetation cover, %); (b) NDVI vs. soil salt content (g/kg); (c) AFII vs. VC; (d) AFII vs. soil salt content (g/kg); n=62.

2.3 The relationship between AFII and SI in feature space

Feature space was constructed based on the assumption presented in Fig. 6a. A negative relationship between AFII and SI is revealed in Fig. 10a. Pixels near the top of the y-axis and the left of the x-axis are al-

tered significantly and present a high risk of soil salinization with high SI and low AFII. Moderately salt-affected soil dominates the middle area of feature space, with salinity increasing from non salt-affected soil to severely salt-affected soil. T_1, T_2, T_3 and T_4 are the mean values of non salt-affected soil, slightly

salt-affected soil, moderately salt-affected soil, and severely salt-affected soil, respectively. There is a negative correlation (R^2=0.6437, Fig. 10b) with 95%

confidence ($P \leq 0.001$) between AFII and SI, in which the greater the distance from T1, the stronger the soil salinization (Fig. 10b).
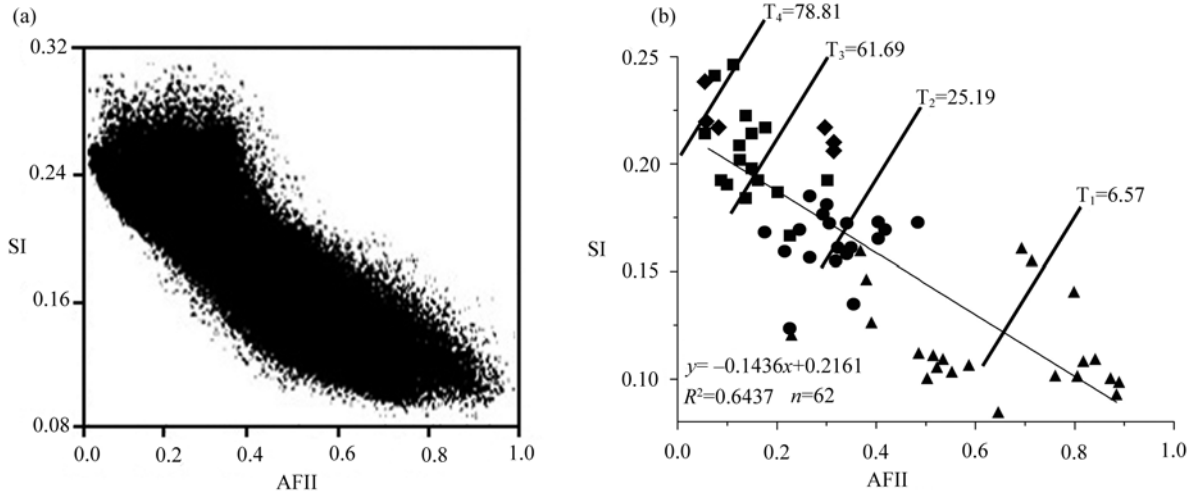

Fig. 10 Construction of two-dimensional feature space using AFII and SI. (a) Scatter plot of AFII and SI from an image of the study area. (b) Relationship between AFII and SI retrieved from the image corresponded with measured data. The individual symbols represent different types of salt-affected soil: triangle (non salt-affected soil), circle (slightly salt-affected soil), square (moderately salt-affected soil), and diamond (severely salt-affected soil).

2.4 Model validation

The K value of –0.1436 in Eq. 9 is the calibration result of the parameter from line AD, which was calculated based on 300 random samples from the TM image of the study area. By introducing K into Eq. 5, the final equation of SDM1 can be written as:

$$SDM1 = \left| \frac{-0.1436Y_{SI} + X_{AFII} - 1}{\sqrt{1 + 0.1436^2}} \right|. \quad (9)$$

The predictive ability of the two models (SDM1 and SDM2) was assessed using ground truth data by comparisons with COSRI. The COSRI is defined as follows:

$$COSRI = \left[(b1 + b2) / (b3 + b4) \right] \times NDVI. \quad (10)$$

Where b1, b2, b3 and b4 are the first four bands of the TM image.

Table 2 summarizes the valuation of the three models (Fig. 11) using the coefficient of determination (R^2) and RSME with respect to the field measurements. It can be seen in Table 2 that two nonlinear relationships, an exponential form (Model A) and a polynomial form (Model B), exist between the soil salt content

and estimated value. Goodness-of-fit performs reasonably well for both Model A and Model B over all participants, including COSRI, SDM1 and SDM2. Among those outcomes (Table 2), there is no marked contrast in overall accuracy between SDM 1 and SDM 2, whether using Model A or Model B. The values of RMSE for SDM 1 were 10.43 with Model A and 11.36 with Model B, and 10.12 with Model A and 11.28 with Model B for SDM2. In contrast, COSRI has a relative high RMSE of 15.10 with Model A and 16.41 with Model B. The coefficients of determination (R^2) between SDM2 and soil salt content are the highest, followed by SDM1 and, finally, COSRI. There-

Table 2 Ability of COSRI, SDM1 and SDM2 to predict soil salinity in exponential and polynomial forms

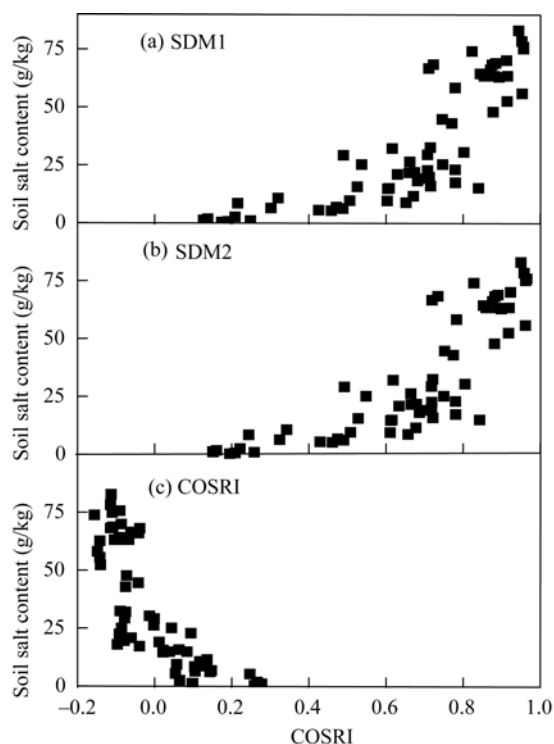|	Model	Equation	R^2	RMSE
COSRI	Model A	$y=18.296e^{-10.131x}$	0.7410	15.10
	Model B	$y=452.49x^2-212.86x+26.155$	0.6540	16.41
SDM1	Model A	$y=0.6285e^{5.1765x}$	0.8134	10.43
	Model B	$y=153x^2-83.403x+12.988$	0.7658	11.36
SDM2	Model A	$y=0.5655e^{5.2757x}$	0.8156	10.12
	Model B	$y=155.22x^2-87.914x+14.296$	0.7708	11.28

Fig. 11 Regression between the three models and soil salt content. (a) SDM1 vs. soil salt content (g/kg); (b) SDM2 vs. soil salt content (g/kg); (c) COSRI vs. soil salt content (g/kg); *n*=62.

fore, exponential models are recommended for estimating soil salt content.

Exponential models were chosen because of their relatively better performance. To further analyze the prediction capability, we performed a contrast analysis on the predicted values of these three models with *in situ* measurements. A total of 30 samples were selected from the field measurements for model validation. These samples are spatially independent of those used as training data for the construction of models mentioned above (32 samples). The results revealed that the coefficient of determination of the soil salt content predicted by the COSRI (R^2>0.718) was lower than that from the SDM1 (R^2>0.867) and SDM2 (R^2>0.865). Soil salt content was predicted by SDM1, and SDM2 well matched the field measurements. RMSEs for SDM1 and SDM2 are 6.86 and 6.97, respectively (Table 3). These results imply a superior

Table 3   Relationship between estimated and measured values

Model	Number of samples	R^2	RMSE
COSRI	30	0.7185	16.21
SDM1	30	0.8673	6.86
SDM2	30	0.8652	6.97

performance of the two new models when compared to COSRI, which illustrates that the SDMs, especially SDM1, were better indicators than the COSRI.

3   Discussion

The study area is demonstrated by a spatially heterogeneous group of saline soils and vegetative cover that is strongly driven by topography. Spatial variability is related to the distribution of soil types (dark soil and light soil) and vegetation communities (crops and halophytes) in the study area. Because of the existence of a spectral mixture of soil and vegetation in pixels in this situation, limitations exist with respect to assessing the soil salt content using remote sensing data directly, such as Landsat images (Metternicht and Zinck, 2003). Therefore, we attempted to utilize the information from vegetation; hence, we considered soil and vegetation simultaneously to detect the soil salt content. Plants can be used to predict soil variables such as the salt content, either from field observations or by remote sensing (Fernandez-Buces et al., 2006), as was also noted in field measurements of soil salt content and vegetation cover in this study (Fig. 7). Therefore, effective and accurate information on certain vegetation as a reflection of the soil salt content is the key factor in evaluating the soil salt content. NDVI shows a positive correlation with photosynthetic activity, biomass and leaf area index, and has proven to be useful in analyzing vegetation patterns and assessing vegetation dynamics. In addition, Brunner et al. (2007) found a relationship (R^2=0.63) between an uncalibrated salinity map (NDVI-based) and field data (soil salinity) during summer in Yanqi Basin, northwestern China. We examined the ability of NDVI to retrieve the soil salt content and vegetation cover from remote sensing in the study area (Figs. 7a and b). However, low vegetation (halophyte that indicates the extent of the soil salt content) density has not been considered explicitly by NDVI, nor has high RMSE been used to retrieve the soil salt content (Fig. 9b). NDVI has low sensitivity to sparse vegetation because of the interference by light soil backgrounds and is an ambiguous indicator for the extent of salinity in arid regions. Therefore, AFII, which is an auxiliary index for the estimation of soil salt content, was established to in-

terpret vegetation cover based on SMA (Fig. 5).

As illustrated in Fig. 9a, soil salinization was analyzed appropriately by AFII (Fig. 9b). The amplitude of change in both vegetation cover and soil salt content was captured better by AFII than by NDVI (Fig. 7). This index achieved a higher accuracy, presumably due to a better representation of intra-class spectral variability. De Asis and Omasa (2007) used a fraction combined with different endmembers to extract vegetation cover based on SMA, achieving a very high correlation coefficient (r=0.94) with field measurements. However, the improvement in AFII was not sufficient enough to accurately estimate the soil salt content compared to retrieving the vegetation cover (Figs. 9c and d). Therefore, the feature space employed AFII and a component of SI and was structured to improve the detection of soil salinity (Fig. 10a).

Increases in soil salt content decrease the greenness of the canopy and increase soil reflectance. Being quite a similar shape to that of Ts-NDVI space, corresponding different SSS was obtained with AFII-SI scatter plot when the axes were substituted with an improved vegetation index and soil salinity index (Fig. 10a). As shown in Fig. 10b, heterogeneous surfaces with different salt-affected soils have further validated the hypothesis presented in Fig. 6a.

Two types of models were developed, including exponential and polynomial forms. The prediction level was improved when the exponential model was used in place of the polynomial model that considers the models proposed here, including COSRI and SDMs. The SDMs showed superior results when compared with the COSRI according to measurements of precision and stability. COSRI was built for a semi-arid environment in Mexico and may not be suitable for arid areas. The ambiguity of NDVI-based models (such as COSRI) for predicting salinity is related to species differences existing in the spectral thresholds and spectral responses to salinity. These differences may originate from the diverse adaptation mechanisms to salinity, such as salt sensitivity (crops) and halophyte characteristics captured by AFII in SDMs according to SMA. This improvement compensates for the limitation of only using soil reflectance. Furthermore, unlike NDVI, which utilizes only the visible and near-infrared bands, the SMA makes use of the full spectral reflectance.

Although soil moisture has been shown to be a major factor controlling soil reflectance, the area we study is almost completely dry because of a high rate of evapotranspiration. In addition, many other physical properties (e.g. surface roughness and organic matter) also influence surface reflectance. This was not considered in the present study. Moreover, the time of image acquisition should be at a specific season when various vegetation species grow, which can relatively indicate the extent of soil salinization at that location. If the proposed method is applied in other arid or semi-arid areas in the future, a map of vegetation types may be needed to better interpret the remote sensing image.

4　Conclusion

Using only the soil spectrum might not meet the request to quantitatively estimate soil salinity. Vegetation as a potential factor may help to improve the accuracy of detecting soil salt content. Our study presented a simple methodology for detecting soil salinity called SDMs, including SDM1 and SDM2. The SDMs were built by combining the spectra of halophytes and bare soil based on a feature space that consists of AFII and SI.

The paper compared six types of remote sensing inversion approaches (COSRI, SDM1 and SDM2 in exponential and polynomial forms) to determine an appropriate model for deriving soil salinity in an arid region. The result found that SDM1 and SDM2 in an exponential form exhibited the highest accuracy. The results of this study validated our assumptions and successfully countered the negative situation in which lower precision in evaluating the soil salt content due to vegetation factors leads to spectral confusion.

It should be noted that AFII is based on the average spectra of halophytes and soil supported by SMA. Further studies should focus on each halophyte separately with a specific spectral mixture model. Another relatively new technique, the multiple-endmember SMA model (MESMA), may also be able to better capture the spectral variability in surface reflectance in heterogeneous salt-affected landscapes.

Acknowledgments

References

Brunner P, Li H T, Kinzelbach W, et al. 2007. Generating soil electrical conductivity maps at regional level by integrating measurements on the ground and remote sensing data. International Journal of Remote Sensing, 28(15): 3341–3361.

Bui E N, Henderson B L. 2003. Vegetation indicators of salinity in northern Queensland. Austral Ecology, 28(5): 539–552.

Camacho-De Coca F, Garcia–Haro F J, Gilabert M A, et al. 2004. Vegetation cover seasonal changes assessment from TM imagery in a semi-arid landscape. International Journal of Remote Sensing, 25(17): 3451–3476.

Carter G A. 1993. Responses of leaf spectral reflectance to plant stress. American Journal of Botany, 80(3): 239–243.

Dehaan R L, Taylor G R. 2002. Field-derived spectra of salinized soils and vegetation as indicators of irrigation-induced soil salinization. Remote Sensing of Environment, 80(3): 406–417.

Douaoui A E K, Nicolas H, Walter C. 2006. Detecting salinity hazards within a semiarid context by means of combining soil and remote-sensing data. Geoderma, 134(1–2): 217–230.

Fernandez-Buces N, Siebe C, Cram S, et al. 2006. Mapping soil salinity using a combined spectral response index for bare soil and vegetation: a case study in the former lake Texcoco, Mexico. Journal of Arid Environments, 65(4): 644–667.

Ghulam A, Qin Q M, Zhan Z M. 2007a. Designing of the perpendicular drought index. Environmental Geology, 52(6): 1045–1052.

Ghulam A, Li Z L, Qin Q, et al. 2007b. Exploration of the spectral space based on vegetation index and albedo for surface drought estimation. Journal of Applied Remote Sensing, 1(1): 1–12.

Gillies R R, Carlson T N, Cui J, et al. 1997. A verification of the 'triangle' method for obtaining surface soil water content and energy fluxes from remote measurements of the Normalized Difference Vegetation Index (NDVI) and surface radiant temperature. International Journal of Remote Sensing, 18(15): 3145–3166.

Green A A, Berman M, Switzer P, et al. 1988. A transformation for ordering multispectral data in terms of image quality with implications for noise removal. IEEE Transactions on Geoscience and Remote Sensing, 26(1): 65–74.

He Q S, Tiyip T, Ding J L. 2006. The extraction of saline soil information in arid area based on decision tree algorithm: a case study in the delta oasis of Weigan and Kuqa Rivers. Resources Science, 28(6): 134–140.

Jiang H, Ding J, Tahiplot T, et al. 2008. Extraction of salinized soil information in arid area based on ETM+ data. Acta Pedologica Sinica, 45(2): 222–228.

Jiapaer G, Chen X, Bao A M. 2011. A comparison of methods for estimating fractional vegetation cover in arid regions. Agricultural

and Forest Meteorology, 151(12): 1698–1710.

Khan N M, Sato Y. 2001. Monitoring hydro-salinity status and its impact in irrigated semi-arid areas using IRS-1B LISS-II data. Asian Journal of Geoinform, 1(3): 63–67.

Khan N M, Rastoskuev V V, Sato Y, et al. 2005. Assessment of hydrosaline land degradation by using a simple approach of remote sensing indicators. Agricultural Water Management, 77(1–3): 96–109.

Luo G P, Lu L, Yin C Y, et al. 2009.An analysis of oasis stability in arid areas: a case study in the northern slope areas of the Tianshan Mountains. Journal of Arid Land,1(1): 49–56.

Metternicht G I, Zinck J A. 2003. Remote sensing of soil salinity: potentials and constraints. Remote Sensing of Environment, 85(1): 1–20.

Montandon L M, Small E E. 2008. The impact of soil reflectance on the quantification of the green vegetation fraction from NDVI. Remote Sensing of Environment, 112(4): 1835–1845.

Mougenot B, Pouget M, Epema G F. 1993. Remote sensing of salt affected soils. Remote Sensing Reviews, 7(3–4): 241–259.

Peterson S H, Stow D A. 2003. Using multiple image endmember spectral mixture analysis to study chaparral regrowth in southern California. International Journal of Remote Sensing, 24(22): 4481–4504.

Rondeaux G, Steven M, Baret F. 1996. Optimization of soil-adjusted vegetation indices. Remote Sensing of Environment, 55(2): 95–107.

Small C, Lu J W T. 2006. Estimation and vicarious validation of urban vegetation abundance by spectral mixture analysis. Remote Sensing of Environment, 100(4): 441–456.

Tilley D R, Ahmed M, Son J H, et al. 2007. Hyperspectral reflectance response of freshwater macrophytes to salinity in a brackish subtropical marsh. Journal of Environmental Quality, 36(3): 780–789.

Vandermeer F. 1995. Spectral unmixing of landsat thematic mapper data. International Journal of Remote Sensing, 16(16): 3189–3194.

Wardlow B D, Egbert S L. 2008. Large-area crop mapping using time-series MODIS 250 m NDVI data: an assessment for the US Central Great Plains. Remote Sensing of Environment, 112(3): 1096–1116.

Xiao J F, Moody A. 2005. A comparison of methods for estimating fractional green vegetation cover within a desert-to-upland transition zone in central New Mexico, USA. Remote Sensing of Environment, 98(2–3): 237–250.

Xu H. 2006. Modification of normalised difference water index (NDWI) to enhance open water features in remotely sensed imagery. International Journal of Remote Sensing, 27(14): 3025–3033.

Yang J X, Wang Y P. 2011. Estimating evapotranspiration fraction by modeling two-dimensional space of NDVI/albedo and day-night land surface temperature difference: a comparative study. Advances in Water Resources, 34(4): 512–518.

Yang Z P, Gao J X, Zhou C P, et al. 2011. Spatio-temporal changes of NDVI and its relation with climatic variables in the source regions of Yangtze and Yellow rivers. Journal of Geographical Sciences, 21(6): 979–993.

Zhang F, Tiyip T, Ding J L. 2012. Spectral reflectance properties of major objects in desert oasis: a case study of the Weigan–Kuqa river delta oasis in Xinjiang, China. Environmental Monitoring and Assessment, 184(8): 5105–5119.